ACS Chemical Neuroscience

Research Article

pubs.acs.org/chemneuro

Modeling the Kinetic Diversity of Dopamine in the Dorsal Striatum

Seth H. Walters, Elaine M. Robbins, and Adrian C. Michael*

Department of Chemistry, University of Pittsburgh, Pittsburgh, Pennsylvania 15260, United States

Supporting Information

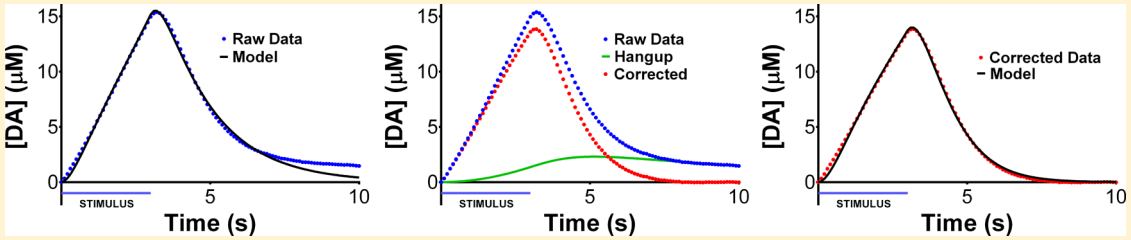

ABSTRACT: Dopamine is an important neurotransmitter that exhibits numerous functions in the healthy, injured, and diseased brain. Fast scan cyclic voltammetry paired with electrical stimulation of dopamine axons is a popular and powerful method for investigating the dynamics of dopamine in the extracellular space. Evidence now suggests that the heterogeneity of electrically evoked dopamine responses reflects the inherent kinetic diversity of dopamine systems, which might contribute to their diversity of physiological function. Dopamine measurements by fast scan cyclic voltammetry are affected by the adsorption of dopamine to carbon fiber electrodes. The temporal distortion caused by dopamine adsorption is correctable by a straightforward mathematical procedure. The corrected responses exhibit excellent agreement with a dopamine kinetic model cast to provide a generic description of restricted diffusion, short-term plasticity of dopamine release, and first-order dopamine clearance. The new DA kinetic model brings to light the rich kinetic information content of electrically evoked dopamine responses recorded via fast scan cyclic voltammetry in the rat dorsal striatum.

KEYWORDS: *Dopamine, voltammetry, kinetic diversity, kinetic model, restricted diffusion*

Dopamine (DA) is an important neurotransmitter in the central nervous system.[1] It contributes to many aspects of healthy brain function[2−4] and plays a central role in multiple neurological[5−8] and psychiatric[9−11] disorders. Fast-scan cyclic voltammetry (FSCV), a popular and powerful method[12−16] for monitoring DA in terminal fields such as the dorsal striatum (DS) and nucleus accumbens (NA), is often paired with electrical stimulation of DA axons in the medial forebrain bundle. Electrical stimulation evokes DA responses that are heterogeneous in amplitude and temporal profile.[17−19] Although often attributed to distortions of the FSCV signal,[20−22] recent evidence suggests that an inherent diversity of DA kinetics contributes to the heterogeneity.[23−29] Such kinetic diversity could well be a contributing factor in DA's functional diversity.

Electrically evoked DA responses are suitable targets for kinetic modeling,[27,30] in part because the timing of the stimulus pulses is known. A kinetic model formulated to describe restricted diffusion reproduces many features of the evoked DA responses produced in the DS.[27] However, the model was not able to account for a feature known as "hang-up", which is the tendency for the DA signal to remain elevated above its baseline after the stimulus ends.[29]

Herein we confirm that hang-up is caused by adsorption of DA to the surface of FSCV electrodes. We introduce a novel but simple correction procedure that mathematically removes the hang-up feature from calibration and in vivo DA responses. The hang-up correction brings the evoked responses and the DA kinetic model into essentially perfect agreement, permitting a full explanation for the kinetic diversity of evoked DA responses from the DS.

RESULTS AND DISCUSSION

DA Adsorption Causes the Hang-Up. The DS produces five statistically distinct evoked DA responses, four fast types and one slow type.[28] All the responses exhibit hang-up, which refers to the tendency of the DA signal to remain elevated above the prestimulus baseline after the stimulus ends.[31] For the purposes of DA kinetic modeling, it is important to know the source of the hang-up feature. We confirm here that the hang-up is caused by the adsorption of DA to FSCV electrodes.

FSCV calibration is routinely performed in a flow system that uses a loop injector to deliver a bolus of DA solution to the FSCV electrode. Neither the sensitivity nor the response time of the FSCV electrode is affected by the fluid flow.[31] When the DA bolus arrives the FSCV signal rapidly rises to a new quasi-steady state with a continued but gentle upward slope (Figure 1, blue line). When the DA bolus ends the FSCV signal rapidly falls but not to the baseline: instead, it hangs-up above the baseline and gently slopes downward. The hang-up is small and

Received: May 5, 2015
Accepted: June 17, 2015
Published: June 17, 2015

DOI: 10.1021/acschemneuro.5b00128
ACS Chem. Neurosci. 2015, 6, 1468−1475

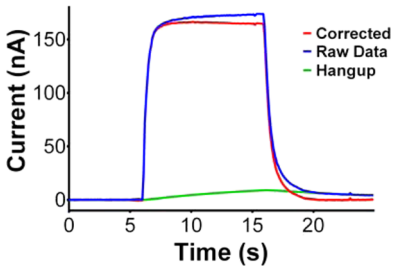

Figure 1. (blue line) In vitro FSCV calibration response to a bolus of 20 μM DA (mean of n = 7 electrodes, SEMs omitted for clarity). (green line) Hang-up component calculated with eq 1. (red line) Corrected calibration response obtained by subtracting the green line from the blue line.

may not always be readily distinguished from noise. However, because the blue line in Figure 1 is the average of responses from n = 7 individual electrodes in a large DA concentration (20 μM), the hang-up is obvious.

To further characterize the hang-up, we exposed n = 7 electrodes to five consecutive 20 μM DA boluses (Figure 2a). The hang-up produces a stepwise increase of the signal in the intervals between each bolus. However, the responses to the individual boluses are superimposable (Figure 2b, the responses are rezeroed to the signal just before the start of each bolus). Additional hang-ups are reported in the Supporting Information document (Figure S1).

The Hang-Up Correction. The persistence of the DA signal after the bolus ends shows that DA remains adsorbed to the electrode surface, as has been documented before.[32,33] The adsorption process exhibits first-order kinetics:[32]

$$\frac{dH}{dt} = k_{on}C - k_{off}\Gamma_{DA} \quad (1)$$

where H represents the hang-up component, k_{on} is the rate constant for adsorption, and k_{off} is the rate constant for desorption. Ideally, C should be the concentration of DA in the solution in close contact with the electrode surface. However, since this concentration is not known independently, we used instead the DA concentration measured by FSCV.

The hang-up component was generated by iteratively adding ($k_{on}C\Delta t$) and subtracting ($k_{off}\Gamma_{DA}\Delta t$) small quantities to H (Δt is the time step). A curve fitting procedure (see Methods) was used to find the best fit of H to the measured hang-up. Finally, the hang-up component was subtracted from the measured response.

Figure 1 illustrates the hang-up correction procedure. The blue line is the measured DA calibration response, the green line is the hang-up component of best-fit to the data segment beginning at t = 20 s and ending at t = 25 s, and the red line is the corrected response obtained by subtraction (red = blue − green). The hang-up correction "squares-up" the response during the DA bolus and "pulls" the response back to baseline after the DA bolus ends.

We applied the hang-up correction in identical fashion to evoked DA responses measured in vivo (Figure 3). The blue

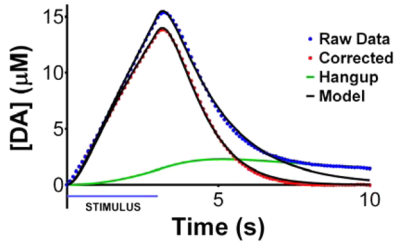

Figure 3. (a) Type 1 fast DS response (blue dots, from ref 28), the hang-up component (green line), and the corrected response (red dots). The solid black lines are the best-fit restricted diffusion models of the in vivo responses, before and after the hang-up correction. The Pearson's correlation coefficient for fit to the corrected response is 0.9990.

symbols in Figure 3 show the type 1 fast response produced in the DS (from Taylor et al.[28]), the green line is the hang-up component of best-fit to the data segment beginning at t = 8 s and ending at t = 10 s, and the red symbols show the corrected response (red = blue − green). The hang-up correction only slightly alters the ascending phase of the response and pulls the descending phase back to the baseline.

To clarify the hang-up correction procedure, eq 1 is used iteratively to generate a calculated hang-up component starting at t = 0 s and running to the end of the measured response. However, only the sum of squares of the residuals in the specified time windows (i.e., 20 s < t < 25 s in Figure 1 and 8 s < t < 10 s in Figure 3) is used to determine the best-fit (see Curve Fitting in the Methods section). We should also mention that the exposure of FSCV electrodes to brain tissue alters their performance, probably via adhesion of proteins and other biomolecules to the electrode surface. The hang-up correction procedure does not involve any assumption that the electrode behaves in the same way during calibration as during in vivo measurements. This is because the correction is applied to each response individually: by this approach, new parameter values

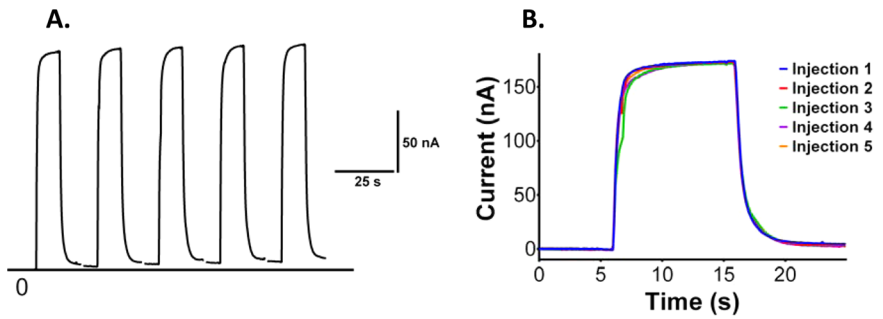

Figure 2. (A) In vitro response to five consecutive DA boluses (20 μM) (average response, n = 7, SEMs omitted for clarity). (B) Five consecutive responses from panel a rezeroed and superimposed.

DOI: 10.1021/acschemneuro.5b00128
ACS Chem. Neurosci. 2015, 6, 1468−1475

and a new hang-up component are determined during calibration and in vivo recording.

The effect of the hang-up correction is similar to that reported in Figure 7 of Bath et al.[32] who compared DA responses recorded by FSCV at scan frequencies varying from 10 to 240 Hz: at 240 Hz there is very little time available for DA adsorption to occur. Increasing the frequency to 240 Hz had minimal effect on the ascending phase of responses recorded in brain slices and in vivo and also "pulled" the descending phase back to the baseline, in similar fashion to the mathematical hang-up correction reported here (Figure 3).

The DA Kinetic Model. The DA kinetic model used in the present study is a slight modification of the one introduced by Walters et al.[27] and previously employed by Taylor et al.,[28] which contains a generic description of restricted diffusion as described by Nicholson and co-workers.[33−35] The model divides the extracellular space into inner and outer compartments and postulates that DA is released into the inner compartment and subsequently transported to the outer compartment, where it is detected by FSCV. The inner and outer compartments are just constructs in the model: they do not necessarily correspond to actual physical compartments in the extracellular space. However, the transport step between the inner and outer compartment effectively and conveniently captures the concept of restricted diffusion. The model is composed of two equations:

$$\frac{\mathrm{dDA_{ic}}}{\mathrm{d}t} = R_p f\ \mathrm{e}^{-k_R t} - \mathrm{DA_{ic}} k_T \quad (2)$$

$$\frac{\mathrm{d[DA]_{oc}}}{\mathrm{d}t} = \frac{\mathrm{DA_{ic}} k_T}{V_{oc}} - [\mathrm{DA}]_{oc} k_U \quad (3)$$

Equations 2 and 3 describe over time the amount (in moles) of DA in the inner compartment, DA_{ic}, and the concentration of DA in the outer compartment, $[DA]_{oc}$, respectively. There are four adjustable parameters; R_P represents the moles of DA released per stimulus pulse, k_R is a first order rate constant that modifies DA release, k_T is a first-order rate constant for transport between the compartments, and k_U is a first-order rate constant for DA uptake. Curve fitting (see Methods) was used to find the values of the adjustable parameters that produce the best fit between the modeled and measured responses. There are two fixed parameters; V_{oc} is the volume of the outer compartment, which is set to 16 μm^3 (see Walters et al),[27] and f is the frequency of the experimental stimulus.

The black lines in Figure 3 report the best fits of the DA kinetic model (eqs 2 and 3) to the as-measured and hang-up corrected type 1 responses (the sum of squares was evaluated beginning at t = 0 s and ending at t = 8 s). The model does not reproduce the hang-up. However, the best fit to the hang-up corrected response is essentially perfect (Pearson's correlation coefficient = 0.9990).

Figure 4 shows the best fits of the DA kinetic model (lines) to the hang-up corrected versions of the five evoked response types from the DS (symbols, data from ref 29; see Supporting Information Figure S2 for the individual hang-up corrections). All the fits are excellent (Pearson's correlation coefficients >0.99) although, as discussed below, there are noticeable differences just after the stimulus begins.

Table 1 lists the values of the four adjustable parameters producing the best fit to each hang-up corrected response type. The parameters R_p and k_U represent the kinetics of DA release and uptake, respectively. In contrast to the more conventional

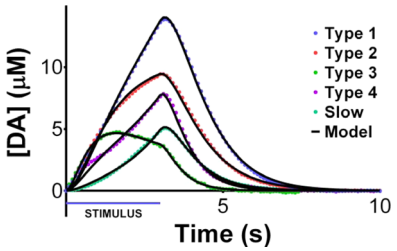

Figure 4. (symbols) Hang-up corrected versions of the five DS evoked responses (raw data from Taylor et al.[28]). (lines) Best fits of the DA kinetic model consisting of eqs 2 and 3 of the text (Pearson's correlation coefficients all exceed 0.99).

Table 1. Parameters from Figure 4

	R_p (zmol)	k_U (s^{-1})	k_T (s^{-1})	k_R (s^{-1})
type 1	3.45	1.29	1.29	−0.24
type 2	5.87	2.02	0.96	0.01
type 3	6.75	3.79	1.86	0.24
type 4	2.96	3.33	1.45	−0.42
slow	0.895	2.52	1.22	−0.67

use of Michaelis−Menten kinetics,[30] our model uses first-order uptake kinetics because the descending phase of the evoked responses exhibit purely first order behavior.[28] The parameter k_T accounts for the mass transport of DA between the inner and outer compartment (restricted diffusion).[27] The parameter k_R is a "short-term plasticity factor" that modifies the rate of DA release: positive values reproduce the short-term depression of fast responses and negative values reproduce the short-term facilitation of hybrid and slow responses.

Hang-Up Correction via Deconvolution is Mathematically Incorrect. Figures 1−3 illustrate that the hang-up correction is an important step in the kinetic modeling of evoked DA responses. Prior attempts to carry out hang-up corrections via deconvolution[22,36,37] have encountered deconvolution artifacts.

Figure 5 shows the type 1 response before (red line) and after (blue line) deconvolution using the exponential response

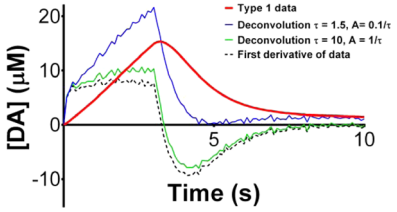

Figure 5. Deconvolution of the type 1 fast DS response (red line, from ref 28) with a time constant of 1.5 s (blue line) and 10 s (green line): the response function is $g(t) = A_0\ \mathrm{e}^{-t/\tau}$ (from ref 37). The numerical derivative of the response is included for comparison (dashed line).

function, $g(t) = A_0\ \mathrm{e}^{-t/\tau}$, and time constant, τ = 1.5 s, from the recent literature.[37] The deconvolution does not remove the hang-up but rather dramatically alters both the ascending and descending phases of the response and accentuates the noise. Increasing τ to 10 s (Figure 5, green line) successfully eliminates the hang up but also converts the ascending phase of the response into a plateau and causes the descending phase to make a negative excursion below the baseline. These rather dramatic effects on the features of the response must be regarded as deconvolution artifacts.[38,39]

DOI: 10.1021/acschemneuro.5b00128
ACS Chem. Neurosci. 2015, 6, 1468−1475

The deconvolution artifacts illustrated in Figure 5 have a sound mathematical explanation. When the time constant is large, the deconvolution result resembles the derivative of the measured response (Figure 5, dashed line). To understand why, it helps to first consider convolution: convolution using the Heaviside step function ($H = 0$ at $t < 0$, $H = 1$ at $t \geq 0$) as the instrument response is mathematically equivalent to integration of the measured response. The instrument response used in the FSCV literature, $g(t) = A_0\ e^{-t/\tau}$, converges on the Heaviside step function as the time constant increases. Consequently, when deconvolution is performed with a large time constant, the result resembles the derivative of the measured response. This explains why hang-up correction via deconvolution leads to mathematical error: FSCV does not record the integral of the DA concentration (see Figure 1).

Dimension of the Diffusion Gap. Prior studies have suggested that evoked DA responses are distorted by a diffusion gap interposed between the FSCV electrode and nearby DA terminals. We show here that any such gap is too small to cause any notable distortion.

In animals treated with a combination of nomifensine (20 mg/kg ip) and raclopride (2 mg/kg ip), FSCV detects DA release evoked by a single stimulus pulse. The time DA needs to reach the electrode can be measured by varying the time between the single stimulus pulse and the next FSCV scan. We varied the time delay in multiples of the 60 Hz period (16.67 ms). DA was detected after 38.33 and 55.00 ms in fast and slow domains, respectively (Figure 6). According to diffusion theory, the average distance of travel, x, of molecules with diffusion coefficient, D, over time interval, t, is

$$x = \sqrt{Dt} \tag{4}$$

Using the reported diffusion coefficient of DA in the rat striatum,[40] $D = 2.4 \times 10^{-6}$ cm^2/s, eq 4 converts these times to distances of 3.0 and 3.6 μm, respectively. Despite their small size, these distances must be taken as *upper* limits, because eq 4 does not account for restricted diffusion. Moreover, these distances are in excellent agreement with the ultrastructure of the DS.[38] Figure 6 strongly supports the point of view that FSCV responses are not distorted by diffusion gaps but rather reflect the kinetic characteristics of DA terminals in close proximity to the recording electrode.[26,28]

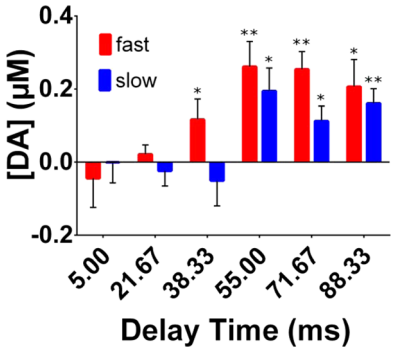

Figure 6. Amplitude of the DA response (mean ± SEM, $n = 7$ rats treated with nomifensine and raclopride) as a function of the delay time between the single stimulus pulse and the next FSCV scan. In fast and slow domains, DA reaches a significant amplitude above zero at 38.33 ms (one-tailed t test: $t(6) = 2.036$, $p < 0.05$) and 55.00 ms (one-tailed t test: $t(6) = 3.116$, $p < 0.05$), respectively. *$p < 0.05$, **$p < 0.005$.

Kinetic Modeling: Two Parameter Sets Produce Identical Results. The restricted diffusion model reproduces some responses with two sets of adjustable parameters (see Supporting Information Table S1). The two parameter sets are related to each other by interchange of the numerical values of k_T and k_U. The R_P parameter tracks k_U: when k_U is larger, R_P is larger, and vice versa. The two parameters sets have the same value of k_R. Thus, the model produces identical results when faster DA kinetics are paired with slower transport as when slower DA kinetics are paired with faster transport. This is not an error in the model: the model does not "know" a priori whether kinetics or transport is rate determining.

To identify the rate-determining step, we modeled responses obtained before and after uptake inhibition with nomifensine (Figure 7). One of the rate constants fell consistently in the range of 1−2 s^{-1} whereas the other was either larger (pre-nomifensine) or smaller (post-nomifensine). We conclude that the nomifensine-independent rate constant is k_T whereas the nomifensine-sensitive rate constant is k_U. This conclusion was used in preparing Table 1.

We were not aware of this issue before now: consequently, we now realize that the k_T and k_U values in Table 2 of Walters et al. (2014)[27] are reversed. A new version of that table is provided in Supporting Information Table S2.

The models in Figure 7 suggest that the slower process, transport or uptake, determines the dynamics of the descending phase of the response. This is because the model postulates that DA transport and DA uptake occur in serial fashion, that is, that transport is a preliminary step in the overall process of uptake. We believe this has profound implications because prior models have postulated that transport and uptake occur in parallel fashion,[30] that is, that diffusion acts to distort the intrinsic DA response. But, if transport and uptake occur in serial fashion, then FSCV measures DA as it diffuses from release sites to uptake sites. This implies that FSCV provides a direct measurement of intrinsic DA.

The Initial Fast Component. The restricted diffusion model provides excellent fits to the hang-up corrected responses (Figure 4). Even so, close inspection of Figure 4 shows that the model consistently underestimates the initial segment of the fast responses (see Figure 8A for an expanded view of the initial segment of Figure 4). It appears that an initial fast component makes an additional contribution to the fast responses just after the stimulus begins.

We modeled the initial fast component with eq 5:

$$DA_{ifc} = A(e^{-k_1 t} - e^{k_2 t}) \tag{5}$$

where A is an amplitude and k_1 and k_2 are rate constants: we reasoned that eq 5 would produce the required curve shape with a minimum number of parameters. We adjusted the three parameters in eq 5 by curve fitting. We used curve fitting to obtain the best fit to the responses upon summation of the initial fast component (eq 5) with the previously determined prolonged component as reported in Figure 4 (i.e., evaluate DA_{ifc} with eq 5, add it to the DA value obtained with eqs 2 and 3, and then evaluate the sum-of-squares of the residuals). Figures 8B and 8C report the best fits (Pearson correlation coefficients >0.996) and the initial fast components, respectively, for each type of fast response. The initial fast component is most obvious in the case of the type 4 hybrid response but all the fast types exhibit this phenomenon. We conclude that the fast responses are composites of initial and prolonged components.

DOI: 10.1021/acschemneuro.5b00128
ACS Chem. Neurosci. 2015, 6, 1468−1475

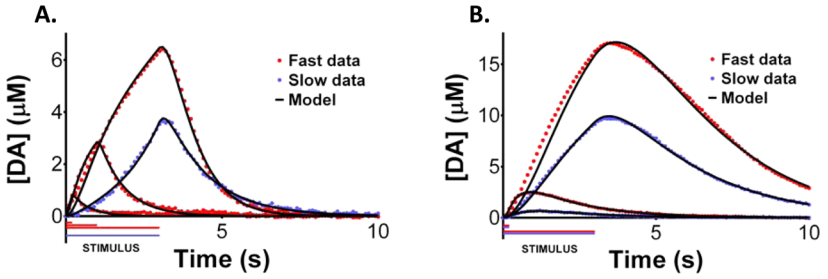

Figure 7. Evoked responses corrected for hang up (symbols) from the fast (red) and slow (blue) domains of the DS from rats before (A) and after (B) treatment with nomifensine (20 mg/kg ip). The lines show the best-fit models: the parameters are reported in the Supporting Information, Table S3. The raw as-measured responses are reported in Figure 5c,d of ref 28.

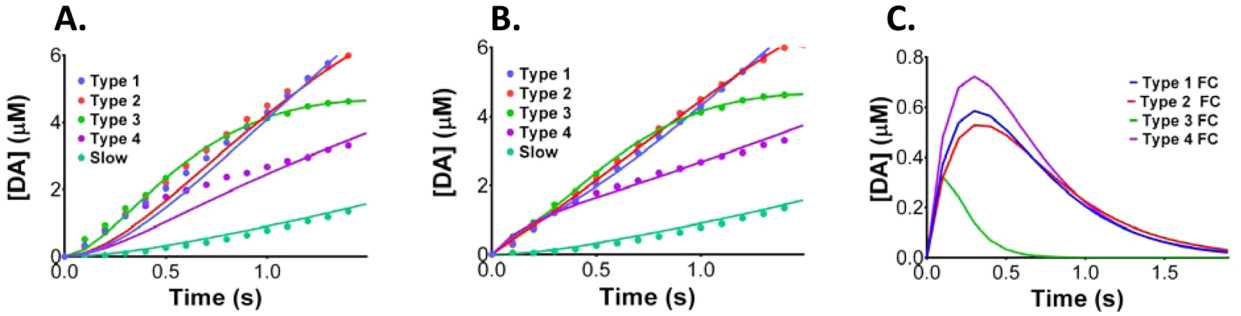

Figure 8. (A) The initial segment of the responses (symbols) and best-fit models (line) from Figure 4 on an expanded scale. (B) The same as panel a with the initial fast components added to the modeled responses. (C) The calculated fast initial components for each type of fast response.

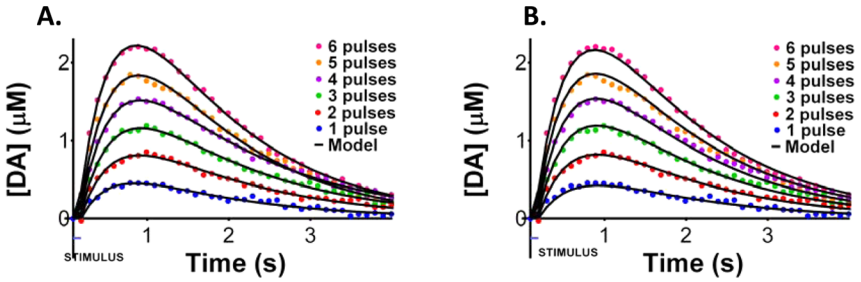

Figure 9. (symbols) Responses evoked by 1−6 stimulus pulses in rats (mean of n = 10, SEMs omitted for clarity) treated with nomifensine (20 mg/kg ip). (lines) Best-fit models. (A) Best-fit models to each evoked response. (B) Single best-fit model to all six evoked responses. The parameters are reported in the Supporting Information, Table S4.

Closer Inspection of the Initial Fast Component. We identified fast DS sites in n = 10 rats. We administered nomifensine, recorded responses evoked by one to six stimulus pulses, and applied the hang-up correction (Figure 9; the raw data are reported in Supporting Information Figure S4). First, we modeled each response individually (Figure 9a; these fits are excellent but the Pearson correlation coefficients are ∼0.96 due to the residual noise). In this case, we set k_R to zero because it had no obvious effect on the quality of the fits, so the fits in Figure 9a were obtained with a three-parameter model. Second, we modeled all six responses simultaneously (Figure 9b, Pearson correlation coefficient 0.96). Thus, Figure 9a shows that the responses can be fit individually with three adjustable parameters, and Figure 9b shows that the entire data set can be modeled with a single set of four adjustable parameters. The parameter values are reported in Supporting Information Table S4.

Figure 9 confirms that the brief stimulus responses exhibit the same overall kinetic behaviors as the prolonged responses in Figure 4. Only the numerical values of the adjustable parameters are different. The k_T values again fall in the consistent 1−2 s^{-1} range. The k_U values are smaller than k_T, an expected consequence of nomifensine administration. The R_p values are ∼10-fold larger than those obtained by modeling the prolonged responses. There may be two reasons for this: first, the responses predominantly represent the initial fast component, and second, uptake inhibition mobilizes DA vesicle pools and promotes DA release.[41]

In the case of the fast domains, the initial fast component might explain our previous observation that the parameters of best fit exhibit a dependence on the duration of the stimulus.[27] The contribution of the initial fast component diminishes as the stimulus proceeds. So, as the duration of the stimulus increases, the kinetic parameters presumably shift from the characteristics of the initial fast component to those of the prolonged component. This trend does not apply to k_T, which falls consistently in the range of 1−2 s^{-1}.

It is tempting to speculate that the initial and prolonged components of the response represent readily releasable and prolonged-release DA vesicle pools,[42] as recently suggested by Zhou and co-workers.[43] Caution is required, however, because we cannot yet eliminate plausible alternatives, such as the

DOI: 10.1021/acschemneuro.5b00128
ACS Chem. Neurosci. 2015, 6, 1468−1475

presence of subpopulations of DA terminals at the recording site or multiple pathways for restricted diffusion to the recording electrode. Future work will be required to clarify this interesting point. Even so, the methods and the kinetic modeling presented here provide access to new information regarding these two components of the DS evoked responses.

The Effect of Uptake on Overshoot. Evoked responses exhibit overshoot, that is, a continued increase in the DA signal after the stimulus ends (the responses in Figure 9 are mostly composed of overshoot). The amplitude and duration of overshoot are sensitive to DAT inhibitors including nomifensine.[24−26,44] Past interpretations of overshoot as a sign of diffusion gaps[21,42] need to be reconsidered given our new data that speak against the presence of diffusion gaps (Figure 6).

The black symbols and line in Figure 10 show the six-pulse stimulus response and best-fit three-paramater kinetic model

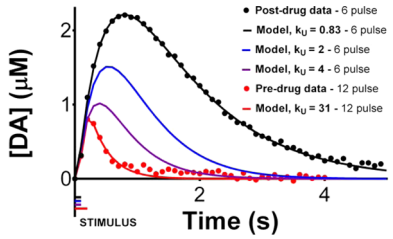

Figure 10. Effect of k_U on overshoot. The six-pulse evoked response from animals treated with nomifensine (black symbols) and its best-fit (black line). Additional responses were modeled by changing only k_U to 2 s^{-1} (blue line) and 4 s^{-1} (purple line). The pre-nomifensine response (red symbols) and best-fit (red line) are included for comparison.

from Figure 9a. The blue and purple lines in Figure 10 show model responses obtained by holding R_p and k_T fixed while increasing k_U to 2 s^{-1} (blue line) and 4 s^{-1} (purple line). Finally, the red symbols and line show a 12-pulse pre-nomifensine response and its best-fit kinetic model. According to Figure 10, decreasing only the value of k_U reproduces the observed tendency of uptake inhibition to increase both the amplitude and duration overshoot (see also Figure 4 of ref 25). No prior DA model has reproduced this tendency solely by adjusting DA uptake kinetics. Thus, Figure 10 is a powerful indicator of the plausibility of our new DA kinetic model.

CONCLUSIONS

This work brings to light the rich kinetic information content of electrically evoked DA responses recorded by in vivo FSCV. The responses include a feature called the hang-up, which arises from the tendency of DA to adsorb to FSCV electrodes. The hang-up feature can be removed by a simple subtraction procedure. The new DA kinetic model, with only four and in some cases only three adjustable parameters, exhibits essentially perfect agreement with the corrected responses (in some cases, with Pearson coefficients exceeding 0.99). By incorporating a novel short-term plasticity factor, k_R, the model accounts for all five types of evoked responses produced in the DS.

This work brings to light an initial component of the fast responses produced in the DS. The origin of this component remains to be identified but possibilities include a readily releasable vesicle pool, a subpopulation of fast-acting DA terminals at the recording sites, and a distribution of restricted diffusion pathways to the FSCV recording electrodes.

Together with previous reports this study establishes that lag and overshoot are kinetic phenomena. Lag is intimately related to autoinhibition, and overshoot is intimately related to uptake. The model reproduces the actions of uptake inhibition on the amplitude and duration of overshoot: this is a powerful indicator of the model's plausibility.

METHODS

Curve Fitting. Curve fitting was used to set the values of the adjustable parameters in the models for the hang-up (eq 1), DA kinetics (eqs 2 and 3), and the initial fast component (eq 5). In each case, a search was conducted for those parameters that produced the best fit between the models and target data as defined by the smallest accessible sum of squares of the residuals, that is, the differences between the modeled and measured data points. The overall quality of the best-fit model was assessed by means of the Pearson correlation coefficient. The search for the best-fit parameters was performed as previously described.[27]

FSCV Procedures. Procedures for FSCV are identical to those described in recent reports from our laboratory.[29] Briefly, carbon fiber electrodes (T650 fibers, Cytec LLC, Piedmont, SC, USA) were 200 μm in length and 7 μm in diameter. The FSCV waveform had a rest potential of 0 V, a positive limit of 1 V, a negative limit of −0.5 V (all vs Ag/AgCl), a sweep rate of 400 V/s, and a repetition frequency of 10 Hz.

In Vitro FSCV Calibration. In vitro FSCV calibration was performed in a homemade flow cell attached to a Rheodyne loop-style low-pressure sample injector valve. Flow was generated by hydrostatic pressure from an elevated reservoir containing N_2-purged artificial cerebrospinal fluid (142 mM NaCl, 1.2 mM $CaCl_2$, 2.7 mM KCl, 1.0 mM $MgCl_2$, 2.0 mM NaH_2PO_4, pH 7.4).

In Vivo Procedures. All procedures involving animals were carried out with the approval of the University of Pittsburgh Animal Care and Use Committee. Several evoked DA responses used herein for modeling are taken from previous publications, which contain the full experimental details.[25,28] The same in vivo procedures were used to obtain the new results in Figures 6, 9, and 10. Briefly, rats (male, Sprague−Dawley, 250−350 g, Charles River Inc., Wilmington, MA) were anesthetized with isoflurane (2.5% by volume O_2), placed in a stereotaxic frame (David Kopf, Tujunga, CA), and connected to an isothermal blanket (Harvard Apparatus, Holliston, MA). Carbon fiber electrodes and stimulating electrodes (MS303/a, Plastics One, Roanoke, VA) were implanted in the dorsal striatum and ipsilateral medial forebrain bundle. Optimization was performed to identify recording sites that produce fast-type evoked responses. The experimental stimulus waveform was a biphasic constant current square wave (2 ms pulses, 60 Hz, 250 μA, 1−6 pulses) delivered with a stimulus isolation unit (Neurolog 800, Digitimer, Letchworth Garden City, UK). Responses evoked by single stimulus pulses were recorded in n = 14 rats treated first with nomifensine (20 mg/kg ip) and then 20 min later with raclopride (2 mg/kg ip): in 7 of these rats recordings were taken at fast sites and in the other 7 rats recordings were taken at slow sites. The time between the single stimulus pulse and the subsequent FSCV scan was varied in increments of 16.67 ms, the period of a 60 Hz stimulus (see Figure 6). Evoked responses were recorded at fast sites in n = 10 rats before and 20 min after the administration of nomifensine (20 mg/kg ip, see Figure 9).

ASSOCIATED CONTENT

Supporting Information

Raw data, without corrections, from which the corrected responses in Figures 4, 8, and 9 were produced and best-fit parameter values for all models except those in Table 1 of the main text. The Supporting Information is available free of charge on the ACS Publications website at DOI: 10.1021/acschemneuro.5b00128.

DOI: 10.1021/acschemneuro.5b00128
ACS Chem. Neurosci. 2015, 6, 1468−1475

AUTHOR INFORMATION

Funding

This work was supported by the NIH (Grant NS086107).

Notes

The authors declare no competing financial interest.

REFERENCES

(1) Carlsson, A., Lindqvist, M., Magnusson, T., and Waldeck, B. (1958) On the presence of 3-hydroxytyramine in brain. *Science 127*, 471.

(2) Claudel, C. E., Cho, M. H., and McDonald, R. D. (1966) Effect of amphetamine and catecholamines on startle response and general motor activity of albino rats. *Nature 210*, 864−865.

(3) Smith, J. E., Co, C., Freeman, M. E., Sands, M. P., and Lane, J. D. (1980) Neurotransmitter turnover in rat striatum is correlated with morphine self-administration. *Nature 287*, 152−154.

(4) Tempel, B. L., Livingstone, M. S., and Quinn, W. G. (1984) Mutations in the dopa decarboxylase gene affect learning in *Drosophila*. *Proc. Natl. Acad. Sci. U. S. A. 81*, 3577−3581.

(5) Turjanski, N., Sawle, G. V., Playford, E. D., Weeks, R., Lammerstma, A. A., Lees, A. J., and Brooks, D. J. (1994) PET studies of the presynaptic and postsynaptic dopaminergic system in Tourette's syndrome. *J. Neurol. Neurosurg. Psychiatry 57*, 688−692.

(6) Chen, J. Y., Wang, E. A., Cepeda, C., and Levine, M. S. (2013) Dopamine imbalance in Huntington's disease: a mechanism for the lack of behavioral flexibility. *Front. Neurosci. 7*, 114.

(7) Starr, M. S. (1996) The role of dopamine in epilepsy. *Synapse 22*, 159−194.

(8) Andén, N. E., Carlsson, A., Kerstell, J., Magnusson, T., Olsson, R., Roos, B. E., Steen, B., Steg, G., Svanborg, A., Thieme, G., and Werdinius, B. (1970) Oral L-dopa treatment of parkinsonism. *Acta Med. Scand. 187*, 247−255.

(9) Carlsson, A. (1977) Does dopamine play a role in schizophrenia? *Psychol. Med. 7*, 583−597.

(10) Shaw, P., Gornick, M., Lerch, J., Addington, A., Seal, J., Greenstein, D., Sharp, W., Evans, A., Giedd, J. N., Castellanos, F. X., and Rapoport, J. L. (2007) Polymorphisms of the dopamine D4 receptor, clinical outcome, and cortical structure in attention-deficit/hyperactivity disorder. *Arch. Gen. Psychiatry 64*, 921−931.

(11) Ritz, M. C., Lamb, R. J., Goldberg, S. R., and Kuhar, M. J. (1988) Cocaine self-administration appears to be mediated by dopamine uptake inhibition. *Prog. Neuropsychopharmacol. Biol. Psychiatry 12*, 233−239.

(12) Ostlund, S. B., Leblanc, K. H., Kosheleff, A. R., Wassum, K. M., and Maidment, N. T. (2014) Phasic Mesolimbic Dopamine Signaling Encodes the Facilitation of Incentive Motivation Produced by Repeated Cocaine Exposure. *Neuropsychopharmacology 39*, 2441−2449.

(13) Brimblecombe, K. R., and Cragg, S. (2015) Ni(2+) affects dopamine uptake which limits suitability as inhibitor of T-type voltage-gated Ca(2+) channels. *ACS Chem. Neurosci. 6*, 124−129.

(14) Cheer, J. F., Wassum, K. M., Sombers, L. A., Heien, M. L. A. V., Ariansen, J. L., Aragona, B. J., Phillips, P. E. M., and Wightman, R. M. (2007) Phasic dopamine release evoked by abused substances requires cannabinoid receptor activation. *J. Neurosci. 27*, 791−795.

(15) Hashemi, P., Dankoski, E. C., Lama, R., Wood, K. M., Takmakov, P., and Wightman, R. M. (2012) Brain dopamine and serotonin differ in regulation and its consequences. *Proc. Natl. Acad. Sci. U. S. A. 109*, 11510−11515.

(16) Huang, E. Y.-K., Tsui, P.-F., Kuo, T.-T., Tsai, J.-J., Chou, Y.-C., Ma, H.-I., Chiang, Y.-H., and Chen, Y.-H. (2014) Amantadine ameliorates dopamine-releasing deficits and behavioral deficits in rats after fluid percussion injury. *PLoS One*, No. e86354, DOI: 10.1371/journal.pone.0086354.

(17) May, L. J., and Wightman, R. M. (1989) Effects of D-2 antagonists on frequency-dependent stimulated dopamine overflow in nucleus accumbens and caudate-putamen. *J. Neurochem. 53*, 898−906.

(18) May, L. J., and Wightman, R. M. (1989) Heterogeneity of stimulated dopamine overflow within rat striatum as observed with in vivo voltammetry. *Brain Res. 487*, 311−320.

(19) Peters, J. L., and Michael, A. C. (2000) Changes in the kinetics of dopamine release and uptake have differential effects on the spatial distribution of extracellular dopamine concentration in rat striatum. *J. Neurochem. 74*, 1563−1573.

(20) Engstrom, R. C., Wightman, R. M., and Kristensen, E. W. (1988) Diffusional distortion in the monitoring of dynamic events. *Anal. Chem. 60*, 652−656.

(21) Kawagoe, K. T., Garris, P. A., Wiedemann, D. J., and Wightman, R. M. (1992) Regulation of transient dopamine concentration gradients in the microenvironment surrounding nerve terminals in the rat striatum. *Neuroscience 51*, 55−64.

(22) Wu, Q., Reith, M. E., Wightman, R. M., Kawagoe, K. T., and Garris, P. A. (2001) Determination of release and uptake parameters from electrically evoked dopamine dynamics measured by real-time voltammetry. *J. Neurosci. Methods 112*, 119−133.

(23) Moquin, K. F., and Michael, A. C. (2009) Tonic autoinhibition contributes to the heterogeneity of evoked dopamine release in the rat striatum. *J. Neurochem. 110*, 1491−1501.

(24) Taylor, I. M., Jaquins-Gerstl, A., Sesack, S. R., and Michael, A. C. (2012) Domain-dependent effects of DAT inhibition in the rat dorsal striatum. *J. Neurochem. 122*, 283−294.

(25) Taylor, I. M., Ilitchev, A. I., and Michael, A. C. (2013) Restricted diffusion of dopamine in the rat dorsal striatum. *ACS Chem. Neurosci. 4*, 870−878.

(26) Shu, Z., Taylor, I. M., Walters, S. H., and Michael, A. C. (2014) Region- and domain-dependent action of nomifensine. *Eur. J. Neurosci. 40*, 2320−2328.

(27) Walters, S. H., Taylor, I. M., Shu, Z., and Michael, A. C. (2014) A Novel Restricted Diffusion Model of Evoked Dopamine. *ACS Chem. Neurosci. 5*, 776−783.

(28) Taylor, I. M., Nesbitt, K. M., Walters, S. H., Varner, E. L., Shu, Z., Bartlow, K. M., Jaquins-Gerstl, A. S., and Michael, A. C. (2015) Kinetic diversity of dopamine transmission in the dorsal striatum. *J. Neurochem. 133*, 522−531.

(29) Shu, Z., Taylor, I. M., and Michael, A. C. (2013) The dopamine patchwork of the rat nucleus accumbens core. *Eur. J. Neurosci. 38*, 3221−3229.

(30) Wightman, R. M., Amatore, C., Engstrom, R. C., Hale, P. D., Kristensen, E. W., Kuhr, W. G., and May, L. J. (1988) Real-time characterization of dopamine overflow and uptake in the rat striatum. *Neuroscience 25*, 513−523.

(31) Venton, B. J., Troyer, K. P., and Wightman, R. M. (2002) Response times of carbon fiber microelectrodes to dynamic changes in catecholamine concentration. *Anal. Chem. 74*, 539−546.

(32) Bath, B. D., Michael, D. J., Trafton, B. J., Joseph, J. D., Runnels, P. L., and Wightman, R. M. (2000) Subsecond adsorption and desorption of dopamine at carbon-fiber microelectrodes. *Anal. Chem. 72*, 5994−6002.

(33) Nicholson, C. (1995) Interaction between diffusion and Michaelis-Menten uptake of dopamine after iontophoresis in striatum. *Biophys. J. 68*, 1699−1715.

(34) Hrabetová, S., and Nicholson, C. (2004) Contribution of dead-space microdomains to tortuosity of brain extracellular space. *Neurochem. Int. 45*, 467−477.

(35) Hrabetová, S., Masri, D., Tao, L., Xiao, F., and Nicholson, C. (2009) Calcium diffusion enhanced after cleavage of negatively charged components of brain extracellular matrix by chondroitinase ABC. *J. Physiol. 587*, 4029−4049.

(36) Atcherley, C. W., Wood, K. M., Parent, K. L., Hashemi, P., and Heien, M. L. (2015) The coaction of tonic and phasic dopamine dynamics. *Chem. Commun. 51*, 2235−2238.

(37) Atcherley, C. W., Laude, N. D., Monroe, E. B., Wood, K. M., Hashemi, P., and Heien, M. L. (2014) Improved calibration of voltammetric sensors for studying pharmacological effects on dopamine transporter kinetics in vivo. *ACS Chem. Neurosci.*, DOI: 10.1021/cn500020s.

DOI: 10.1021/acschemneuro.5b00128
ACS Chem. Neurosci. 2015, 6, 1468−1475

(38) Helene, O., Vanin, V. R., Guimarães-Filho, Z. O., and Takiya, C. (2007) Variances, covariances and artifacts in image deconvolution. *Nucl. Instrum. Methods Phys. Res., Sect. A 580*, 1466−1473.
(39) Smeller, L., Goossens, K., and Heremans, K. (1995) How to minimize certain artifacts in Fourier self-deconvolution. *Appl. Spectrosc. 49*, 1538−1542.
(40) Nicholson, C., and Rice, M. E. (1991) Diffusion of ions and transmitters in the brain cell microenvironment, in *Volume Transmission in the Brain* (Fuxe, K., and Agnati, L. F., Eds.) pp 279−294, Raven Press, New York.
(41) Venton, B. J., Seipel, A. T., Phillips, P. E. M., Wetsel, W. C., Gitler, D., Greengard, P., Augustine, G. J., and Wightman, R. M. (2006) Cocaine increases dopamine release by mobilization of a synapsin-dependent reserve pool. *J. Neurosci. 26*, 3206−3209.
(42) Neher, E. (1998) Vesicle pools and Ca 2+ microdomains: new tools for understanding their roles in neurotransmitter release. *Neuron 20*, 389−399.
(43) Wang, S. R., Yao, W., Huang, H. P., Zhang, B., Zuo, P. L., Sun, L., Dou, H. Q., Li, Q., Kang, X. J., Xu, H. D., Hu, M. Q., Jin, M., Zhang, L., Mu, Y., Peng, J. Y., Zhang, C. X., Ding, J. P., Li, B. M., and Zhou, Z. (2011) Role of vesicle pools in action potential pattern-dependent dopamine overflow in rat striatum in vivo. *J. Neurochem. 119*, 342−353.
(44) Jones, S. R., Garris, P. A., and Wightman, R. M. (1995) Different effects of cocaine and nomifensine on dopamine uptake in the caudate-putamen and nucleus accumbens. *J. Pharmacol. Exp. Ther. 274*, 396−403.

DOI: 10.1021/acschemneuro.5b00128
ACS Chem. Neurosci. 2015, 6, 1468−1475